
Explaining Concept Shift with Interpretable Feature Attribution

Ruiqi Lyu

School of Computer Science
Carnegie Mellon University
ruiqil@cs.cmu.edu

Alistair Turcan

School of Computer Science
Carnegie Mellon University
aturcan@cs.cmu.edu

Bryan Wilder

School of Computer Science
Carnegie Mellon University
bwilder@cs.cmu.edu

Abstract

Regardless the amount of data a machine learning (ML) model is trained on, there will inevitably be data that differs from their training set, lowering model performance. Concept shift occurs when the distribution of labels conditioned on the features changes, making even a well-tuned ML model to have learned a fundamentally incorrect representation. Identifying these shifted features provides unique insight into how one dataset differs from another, considering the difference may be across a scientifically relevant dimension, such as time, disease status, population, etc. In this paper, we propose SGShift, a model for detecting concept shift in tabular data and attributing reduced model performance to a sparse set of shifted features. SGShift models concept shift with a Generalized Additive Model (GAM) and performs subsequent feature selection to identify shifted features. We propose further extensions of SGShift by incorporating knockoffs to control false discoveries and an absorption term to account for models with poor fit to the data. We conduct extensive experiments in synthetic and real data across various ML models and find SGShift can identify shifted features with AUC > 0.9 and recall $> 90\%$, often 2 or 3 times as high as baseline methods.

1 Introduction

Machine learning (ML) models are often trained on vast amounts of data, but will inevitably encounter test distributions that differ from the training set. Such distribution shift is one of the most common failure modes for ML in practice. When models do fail, model developers need to diagnose and correct the problem. In the simplest case, this may simply consist of gathering more data to retrain the model. However, in other cases, it may be necessary to fix issues in an underlying data pipeline, add new features to replace ones that have become uninformative, or undertake other more complex interventions. A necessary starting point for any such process is to understand what changed in the new dataset. Developing such understanding may even have scientific importance. For instance, a novel virus variant may emerge with new risk factors, lowering the performance of models that predict disease progression, or specific mutations in the genome could have differing relevance to disease between ancestries, weakening polygenic risk score models due to fundamentally different biology between populations.

We propose methods for diagnosing distribution shift, focusing specifically on the case of *concept shift*, or when the conditional distribution of the label given the features, $p(y|X)$, differs between the source and target distribution. Concept shift represents the difficult case where the relationship between features and outcome has changed, as opposed to marginal shifts impacting only X or y by themselves. Indeed, [LWCN24] document concept shift as the primary contributor to performance degradation across a wide range of empirical examples of distribution shifts. In this setting, our goal is to understand how $p(y|X)$ differs between the source and target domains.

Little existing work addresses the task of understanding distribution shift. A great deal of previous work aims to develop models that are robust to shift, or which can be quickly adapted using limited samples. Another line of work aims to detect whether shift is present at all, but not to diagnose its cause. Perhaps the closest related work is that of Kulinski et al [KI23]. However, they consider an unsupervised setting where the goal is to identify a set of features whose distribution differs (e.g., sensors that have been compromised by an adversary), as opposed to identifying features whose relationship with a supervised label has changed.

To address this need, we propose SGShift, a framework using Sparse Generalized Additive Models to explain Concept Shift in tabular datasets. Just as sparsity is an effective principle for learning predictive models in many settings, we hypothesize that the *update* to $p(y|X)$ between the source and target domains may often be sparse (a fact that we empirically verify in several application domains). In this case, a useful explanation of concept shift is to identify a small set of features that drive the change between the two distributions, which could e.g. be the subject of potential modeling fixes. SGShift fits a generalized additive model (GAM) as a sparse update term to the source distribution predictive model and then performs feature selection to identify a subset of variables responsible for the difference between source and target distributions. This strategy has several advantages. First, the GAM term that represents the model update is easily interpretable, even if the base model for the source domain is black-box. Second, we show that standard feature selection strategies like ℓ_1 regularization or knockoffs extend naturally to our setting. Third, the simplicity of the update term allows it to perform well at identifying shifted features even with limited samples from the target distribution, as we empirically demonstrate.

We benchmark SGShift against several baselines and synthetic datasets with known feature shifts, observing greatly superior performance at identifying shifted features. We further apply SGShift to real data and recover real-world concept shifts consistent with findings from medical literature. We summarize our main contributions as follows.

1. We propose a sparsity-based model for attributing reduced model performance to conditional distribution shift of specific features. No existing method aims to attribute exactly what features contribute to this shift.
2. We construct extensions to SGShift’s feature selection, showing knockoffs can rigorously control false discoveries.
3. We show a comprehensive empirical study of our methods. On real and semi-synthetic data with natural concept shift, SGShift typically achieves $\text{AUC} > 0.9$ at detecting shifted features, far higher than baseline methods.

2 Related Work

Much of the existing work on distribution shift has focused on detecting or correcting shifts in the marginal feature distribution, $P(X)$, e.g. covariate shift with the assumption that $P(y|X)$ remains unchanged. For instance, [KB120] introduce statistical tests to identify which variables have shifted between source and target domains, while [KI23] propose explaining observed shifts via a learned transportation map between the source and target distributions, not distinguishing between features and labels. $P(X)$ shift can be identified by methods like two-sample tests [JPLB22] or classifiers [LWS18] and corrected by techniques such as importance sampling [SKM07]. Cai et al. [CNY23] further use these ideas to correct covariate shift by regarding the unexplained residual as a shift in $P(y|X)$, although they don’t correct or explain the concept shift.

Although these methods can be effective for addressing covariate shift, they often do not delve into potential shifts in the conditional distribution. Explaining shifts in $P(y|X)$ typically involves performing feature-by-feature analyses of the conditional distribution $P(y|X_i)$ [GMR⁺18]. However, such univariate assessments risk detecting spurious shifts due to unadjusted confounding in the presence of collinearity among predictors [RWY10].

Recent efforts have begun to tackle shifts in the conditional distribution $P(y|X)$ more directly. For example, [ZSGJ23] consider changes in a causal parent set as a whole, although their approach relies on known causal structures. Similarly, [MBM⁺23] propose a model-agnostic “explanation shift detector” that applies SHAP (Shapley additive explanations) to a source-trained model and covariates in both source and target domains, without including the outcomes in the target domain.

They then use a two-sample test on the feature-attribution distributions from SHAP to detect whether the model’s decision logic has changed because of the changing of $P(X)$ across domains. Despite its effectiveness in signaling shifts, this approach does not pinpoint which features are driving the changes in $P(y|X)$ nor does it incorporate the target domain’s outcome variables in a structured way.

Some sparsity-based methods explicitly address collinearity and partial associations by estimating which features exhibit a shift conditional on other features. [CZZ22] introduce the Sparse Joint Shift (SJS) framework, unifying covariate and label shift with a sparse model to estimate performance shift on an unlabeled dataset. While this can output features relevant to shift, without knowing target labels requires restrictive assumptions for identifiability, particularly that non-shifted features have no shifts at all when conditioned on the shifted features and label between datasets. WhyShift [LWCN23] compares two independently trained models - one from each domain - and analyze their difference to locate regions of covariate space with the largest predictive discrepancy. To the best of our knowledge, this work is the only directly comparable method to our framework.

3 Preliminaries

3.1 Problem statement

We consider a standard machine learning prediction task, aiming to use features X to predict label y . For the i -th subject, we observe an outcome variable $y_i \in \mathbb{R}$ and a set of p predictors $X_i \in \mathbb{R}^p$, including the intercept term. A model is trained on labeled source dataset S and is updated to fit target dataset T . A conditional distribution shift occurs between S and T such that $P_S(y|X) \neq P_T(y|X)$. Our goal is to identify the set of features $A \subseteq X$ that result in this shift.

3.2 Conditional distribution shift

We assume the target data $\{X_i, y_i\}$ under the source distribution S is generated as

$$g(\mathbb{E}_S(y_i | X_i)) = f(X_i)$$

where $g(\cdot)$ is a canonical link function determined by the distribution assumption for the response variable (Gaussian, Binomial, etc.), and $f(X_i)$ is the true conditional mean after applying the link function.

We assume the difference between $g(\mathbb{E}_S(y_i | X_i))$ and $g(\mathbb{E}_T(y_i | X_i))$ can be modeled by linear combinations of K fixed basis functions. We note that while this will require an approximation with trained working model \hat{f} which converges to f , we empirically show strong performance even when this assumption falters. Under the target distribution T , a shift occurs so that

$$g(\mathbb{E}_T(y_i | X_i)) = f(X_i) + \phi(X_i)^\top \delta$$

where basis function $\phi(X_i) = [\phi_1(X_i), \dots, \phi_K(X_i)]^\top$ and $\delta \in \mathbb{R}^K$ is sparse. For simplicity, we denote $\phi(X_i)$ as ϕ_i . We seek to identify the set of shifted functions $A = \{j : \delta_j \neq 0\}$.

Given the assumption of the exponential family distribution to generate the dependent variable y , $f(X_i)$ determines the $\mathbb{E}[y_i | X_i]$ under S , and δ captures the shift, with support $A \subseteq [K]$. The negative log-likelihood function of δ can be written as

$$L(\delta) = \sum_i \left\{ \psi(f(X_i) + \phi_i^\top \delta) - y_i(f(X_i) + \phi_i^\top \delta) \right\}$$

where $\psi(\cdot)$ is uniquely determined by the link $g(\cdot)$. We can now attempt to solve for δ to minimize this loss and find which features need updated in T from S .

3.3 Generalized additive models

GAMs [Has17] provide a structured and interpretable approach to describing $P(y|X)$. Its explainability enables the model to be closely monitored and adjusted in the presence of potential distribution shift [MDSR25]. By adding domain-specific components for potentially shifted features, one can naturally disentangle main effects from additional shifts unique to the target domain.

We reformat this as a regression problem for δ in the GAM framework. We specify an exponential family distribution for y and a link $g(\cdot)$, so that under T with sample size n_T , the associated GAM loss is

$$L(\delta) = \sum_{i=1}^{n_T} \ell(y_i, f(X_i) + \phi_i^\top \delta)$$

A GAM model may now be used to solve for δ such that this loss is minimized.

4 Method

We first define a simple model using an ℓ_1 penalty on a GAM to prioritize shifted features (SGShift). We then extend this to account for models that have learned poor representations of the data through an absorption term (SGShift-A). We lastly introduce a more sophisticated feature selection routine by using knockoffs (SGShift-K), which can be combined with the absorption model (SGShift-KA).

4.1 SGShift: ℓ_1 -Penalized GAM

We regularize the GAM loss with an ℓ_1 -penalty

$$\begin{aligned} \hat{\delta} &= \arg \min_{\delta \in \mathbb{R}^K} \left\{ \underbrace{\sum_{i=1}^{n_T} \ell(y_i, \hat{f}(X_i) + \phi_i^\top \delta)}_{\text{GAM Loss}} + \underbrace{\lambda \|\delta\|_1}_{\ell_1\text{-Regularization}} \right\} \\ &= \arg \min_{\delta \in \mathbb{R}^K} \left\{ L(y_T, \hat{f}(X_T) + \phi_T^\top \delta) + \lambda \|\delta\|_1 \right\} \end{aligned}$$

where $\lambda > 0$ is the regularization parameter. Intuitively, the features selected after this regularization are those most strongly contributing to the conditional distribution shift.

We prove a convergence guarantee for estimation error for GAMs similar to common practices of ℓ_1 regularization in Generalized Linear Models (GLMs). We adapt the usual analysis of the lasso estimator for feature selection to accommodate using the regularized component of the model as a correction term to an existing model \hat{f} . For simplicity, let $L(\delta) = L(y_T, \hat{f}(X_T) + \phi_T^\top \delta) = \sum_{i=1}^{n_T} \ell(y_i, \hat{f}(X_i) + \phi_i^\top \delta)$. Let $\delta^* \in \mathbb{R}^K$ be the true parameter with support $A \subseteq [K]$, $|A| = a$, meaning that $\delta_j^* = 0$ for all $j \in A^c$ (where A^c denotes the complement of A). With the assumption that $\phi_i \in \mathbb{R}^K$ is i.i.d. sub-Gaussian vectors with covariance $\Sigma \succ 0$, and $\ell(y, \eta)$ is twice-differentiable and $\nabla_\eta^2 \ell(y, \eta) \geq \kappa > 0$ uniformly, the estimation is guaranteed to converge.

Theorem 4.1 (Convergence Guarantee for Estimation Error Under RSC). *Suppose (1) Restricted Strong Convexity (RSC): $L(\mathbf{a}) - L(\mathbf{b}) - \langle \mathbf{a} - \mathbf{b}, \nabla L(\mathbf{b}) \rangle \geq c_1 n_T \|\mathbf{a} - \mathbf{b}\|_2^2 - c_2 \|\mathbf{a} - \mathbf{b}\|_1^2 \quad \forall \mathbf{a}, \mathbf{b}$. (2) Subgradient Bound: $\|\nabla L(\delta^*)\|_\infty \leq c_3 \lambda$. (3) Regularization Parameter: $n_T \lambda = \lambda' \asymp \sqrt{\log K / n_T}$. Then, with probability approaching 1, the estimation error $\hat{\delta} - \delta^*$ satisfies $\|\hat{\delta} - \delta^*\|_2^2 \leq \frac{C a \log K}{n_T}$, where $C > 0$ depends on c_1, c_2, c_3 but not on n_T, a , or K .*

4.2 SGShift-A: SGShift with absorption of model misspecification

Prioritizing shifted features relies on an existing model trained on the source dataset. However, it may be that this model does not represent the data well due to difficulties in model fitting. To account for misspecification in model fit to the data, we introduce an additional term to absorb this difference. We now incorporate source data and adopt a difference-in-difference structure with parameters (ω, δ) . Suppose we have n_S points from the source (X_S, y_S) and n_T points from the target (X_T, y_T) . The *absorption* idea is that ω appears in *both* source and target, while δ appears *only* in the target domain. Thus, we solve

$$(\hat{\omega}, \hat{\delta}) = \arg \min_{\omega, \delta \in \mathbb{R}^K} \left\{ L \left(\begin{bmatrix} y_S \\ y_T \end{bmatrix}, \underbrace{\begin{bmatrix} \hat{f}(X_S) \\ \hat{f}(X_T) \end{bmatrix}}_{\text{offset}} + \underbrace{\begin{bmatrix} \phi_S^\top & \mathbf{0} \\ \phi_T^\top & \phi_T^\top \end{bmatrix} \begin{bmatrix} \omega \\ \delta \end{bmatrix}}_{\text{absorption}} \right) + \lambda_\omega \|\omega\|_1 + \lambda_\delta \|\delta\|_1 \right\}$$

where $\omega \in \mathbb{R}^K$ acts on both domains and $\delta \in \mathbb{R}^K$ is target-specific. δ captures extra shifts unique to the target, while ω absorbs the main source plus target mismatch. We induce hierarchical regularization $\lambda_\omega < \lambda_\delta$ to penalize the inference of concept shift more heavily than model misspecification to avoid spurious shifted features resulting from poor model fit.

We define the source loss $L_S(\omega)$ and target loss $L_T(\omega, \delta)$ as:

$$L_S(\omega) = \sum_{i \in S} \ell(y_i, \hat{f}(X_i) + \phi_i^\top \omega), \quad L_T(\omega, \delta) = \sum_{i \in T} \ell(y_i, \hat{f}(X_i) + \phi_i^\top (\omega + \delta)),$$

The absorption estimator solves:

$$(\hat{\omega}, \hat{\delta}) = \arg \min_{\omega, \delta} \{L_S(\omega) + L_T(\omega, \delta) + \lambda_\omega \|\omega\|_1 + \lambda_\delta \|\delta\|_1\}.$$

4.3 SGShift-K: SGShift with knockoffs to control false discoveries

Knockoffs are a powerful method for feature selection and false discovery control, generating synthetic features that mimic the correlation structure of the real ones while being conditionally independent of the response variable. Knockoff-based methods can refine the discrete feature selection step with corresponding false discovery control. Following [CFJL18], we create a Model-X knockoff matrix $\tilde{X} = [\tilde{X}^{(1)}, \dots, \tilde{X}^{(p)}] \in \mathbb{R}^{n \times p}$ of a matrix constructed by horizontally stacked random vectors $X = [X^{(1)}, \dots, X^{(p)}] \in \mathbb{R}^{n \times p}$.

Having constructed the knockoffs, we can proceed by applying our variable selection procedure on the augmented design matrix containing both original values of basis functions and knockoffs $[\phi \ \tilde{\phi}] = [\phi(X) \ \phi(\tilde{X})] \in \mathbb{R}^{n \times 2K}$.

We form a coefficient vector $\delta' = \begin{bmatrix} \delta \\ \tilde{\delta} \end{bmatrix} \in \mathbb{R}^{2K}$ similar to how original knockoffs work, but fitting the differences with an offset rather than the original features. We then minimize

$$\delta' = \arg \min_{\delta' \in \mathbb{R}^{2K}} \left\{ L(y_T, \hat{f}(X_T) + [\phi_T \ \tilde{\phi}_T]^\top \delta') + \lambda \|\delta'\|_1 \right\}$$

We then follow the standard knockoffs procedure for selecting features. For each $k = 1, \dots, K$, we compute statistics Z_k and \tilde{Z}_k measuring the importance of X_k and \tilde{X}_k , respectively, in predicting y . Then, we compute the knockoff statistics W_k such that W_k indicates that X_k appears to be more important than its own knockoff copy. The selection of X_k is based on W_k accordingly. For more details, see appendix.

The selection procedure involves two sources of randomness: (1) finite-sample variability inherent to the observed data, and (2) stochasticity in knockoff generation. While the former is irreducible, the latter can be mitigated through stability selection [MB10, RWC23]. Specifically, we derandomize the knockoff filter by aggregating results over B knockoff realizations, expanding upon [RWC23] by controlling the false discovery rate (FDR) in addition to the per-family error rate (PFER) by proving the upper bounds on FDR and PFER (Lemma 4.2). We then follow the derandomized knockoffs procedure. For each $b = 1, \dots, B$, we generate knockoffs $\tilde{X}^{[b]}$ conditional on X , and compute knockoff statistics $W_k^{[b]}$ for $k \in [K]$. Thus, we obtain a knockoff filter's selection set $\hat{A}^{[b]} = \{k : W_k^{[b]} \geq \tau\}$, where τ is the knockoff threshold controlling the per-iteration FDR or PFER.

The aggregated selection frequency for feature k is $\hat{\Pi}_k = \frac{1}{B} \sum_{b=1}^B \mathbf{1}\{k \in \hat{A}^{[b]}\}$, where Π is a user-determined parameter from the derandomized knockoffs procedure [RWC23]. The stability selection set becomes

$$\hat{A}(\pi) = \left\{ k : \hat{\Pi}_k \geq \pi \right\}, \quad \pi \in (0, 1).$$

With stability selection, we can control either per-family error rate (PFER) or false discovery rate (FDR) accordingly, depending on the need. With identical guarantees to the existing PFER control in existing derandomized knockoffs [RWC23], we prove control when fitting the differences between two models. We then extend this proof to further guarantee FDR control.

Lemma 4.2 (Stability Selection Control). *Let $A^c = \{k : \delta_k = 0\}$ denote the set of null features.*

(PFER Control) *Assume for each $k \in A^c$, $P(k \in \hat{A}^{[b]}) \leq \alpha$ uniformly over b , where α is the per-iteration false selection probability controlled via τ . For any stability threshold $\pi > \alpha$:*

$$\mathbb{E} \left[|\hat{A}(\pi) \cap A^c| \right] \leq |A^c| \exp(-2B(\pi - \alpha)^2).$$

(FDR Control) *Assume each $\hat{A}^{[b]}$ satisfies $\mathbb{E} \left[\frac{|\hat{A}^{[b]} \cap A^c|}{|\hat{A}^{[b]}| \vee 1} \right] \leq q$ (FDR control at level q via τ) as per Theorem 3.1 in [CFJL18]. Then:*

$$FDR(\hat{A}(\pi)) \leq \frac{q}{1 - (1 - \pi)^B}.$$

4.4 SGShift-KA: SGShift with knockoffs and absorption

Combining all of the techniques introduced so far, we can add an additional absorption of misspecification to the SGShift-K, named SGShift-KA. Similarly, we form a coefficient vector $\delta' = \begin{bmatrix} \delta \\ \tilde{\delta} \end{bmatrix} \in \mathbb{R}^{2K}$ and $\omega \in \mathbb{R}^K$ to absorb the mismatch, then minimize

$$(\hat{\omega}, \hat{\delta}') = \arg \min_{\omega, \delta'} \left\{ L \left(\begin{bmatrix} y_S \\ y_T \end{bmatrix}, \begin{bmatrix} \hat{f}(X_S) \\ \hat{f}(X_T) \end{bmatrix} + \begin{bmatrix} \phi_S^\top & \mathbf{0} & \mathbf{0} \\ \phi_T^\top & \phi_T^\top & \tilde{\phi}_T^\top \end{bmatrix} \begin{bmatrix} \omega \\ \delta \\ \tilde{\delta} \end{bmatrix} \right) + \lambda_\omega \|\omega\|_1 + \lambda_\delta \|\delta'\|_1 \right\}$$

where $\lambda_\omega < \lambda_\delta$, to again focus more on concept shift rather than differences in model fit.

5 Experiments

Data overview We evaluate our method on three real-world healthcare datasets exhibiting natural distribution shifts (Table 1), 30-day Diabetes Readmission [SDG⁺14], COVID-19 Hospitalizations [oURPI19], and SUPPORT2 Hospital Expenses [CDD⁺95]. SUPPORT2 has a continuous outcome, and the others are binary. Domain splits reflect population, temporal, or outcome differences. Full preprocessing details for each dataset are in the appendix. Code for replication is available in the supplementary material. The datasets are also available, excluding restricted COVID Hospitalization data from All of Us [oURPI19] Registered Tier, where we provide code for fetching the data.

	Diabetes readmission	COVID-19	SUPPORT2
Total samples	73,615	16,187	9,105
Features	33	30	64
Source size	49,213	11,268	5,453
Target size	24,402	2,219	1,817
Domain split	Emergency room admission	New variant	Death in hospital

Table 1: Dataset summary.

Simulation setting We construct semi-synthetic simulations across all three datasets to preserve real-world feature correlations and enable performance comparison given ground truth shifted features. The source and target domain splits are the same as defined in Table 1. We fit a "generator" model to the real labels in the source domain and relabel the source data, and then simulate the target dataset's labels with an induced conditional shift by perturbing $g(E[y|X])$ through additive transformations based on selected input features. This alters the relationship between inputs and labels while keeping the joint distributions of covariates, $P_S(X)$ and $P_T(X)$, the same as the real data. A "base" model is then trained from the relabeled source domain. Model misspecification occurs when the generator and base model classes are mismatched (not identical).

Baselines In absence of directly comparable methods, we construct and adapt 3 baseline models. 1) Diff, a method we construct where we simply compute the outcome discrepancies of two "base models" separately trained on source and target data, and apply sparse regression on held-out samples

and the base models' outcome probability differences to identify features contributing to the shifts. 2) WhyShift [LWCN23] uses two "base models" separately trained on source and target domains and computes model outcome probability discrepancies, then trains a non-linear decision tree on these discrepancies to detect regions (paths in the tree) responsible for conditional shifts. We extract the features from any path in the learned tree with feature importance > 0 and consider them as the shifted features. 3) SHAP, a Shapley value-based method we adapt from [MBM⁺23] such that we can find individual features that differ between datasets. SHAP trains "base models" separately on source and target data, computes the Shapley value of each feature, and ranks the largest absolute differences between models.

Model configurations We evaluate our framework's performance across a diverse set of machine learning models. For classification tasks, we employ logistic regression, decision trees, support vector machines (SVM), and gradient-boosted trees. For regression tasks, we consider linear regression, regression trees, SVM regressors, and gradient-boosting regressors. All models use scikit-learn with hyperparameters provided in the appendix. Every combination of model configurations of generator and base models (16 total) is considered in simulations for each dataset.

6 Results

Evaluation Table 2 shows evaluation of SGShift in detecting shifted features in semi-synthetic simulations, measured in AUC at detecting true shifted features (a binary 0/1 label), and recall of the same task, evaluated at fixed FPR 10%. We show aggregated results in both the matched setting, where generator and base model are identical, and mismatched, where they differ and the base model is misspecified. Across model settings and datasets, we observe much stronger performance for the variations of SGShift compared to baselines Diff, WhyShift and SHAP, with AUC typically 0.1-0.2 higher. Incorporating knockoffs with SGShift-K and SGShift-KA often leads to AUC greater than 0.9. Adding the absorption term to SGShift with and without knockoffs increases performance in nearly every setting, especially recall. SGShift-KA often discovers more than 80-90% of the true shifted features. Individual model configuration results are available in appendix.

Model Match	AUC / Recall						
	SGShift	SGShift-A	SGShift-K	SGShift-KA	Diff	WhyShift	SHAP
Diabetes Readmission							
Matched	0.80 / 0.42	0.81 / 0.50	0.90 / 0.82	0.90 / 0.81	0.64 / 0.27	0.73 / 0.29	0.77 / 0.34
Mismatched	0.79 / 0.43	0.81 / 0.50	0.84 / 0.66	0.86 / 0.71	0.69 / 0.33	0.72 / 0.30	0.76 / 0.30
COVID-19							
Matched	0.86 / 0.50	0.88 / 0.56	0.99 / 0.97	0.95 / 0.90	0.78 / 0.33	0.76 / 0.41	0.81 / 0.59
Mismatched	0.85 / 0.47	0.87 / 0.54	0.97 / 0.89	0.95 / 0.84	0.77 / 0.28	0.71 / 0.33	0.77 / 0.46
SUPPORT2							
Matched	0.92 / 0.83	0.94 / 0.82	0.96 / 0.95	0.96 / 0.96	0.83 / 0.64	0.67 / 0.40	0.82 / 0.70
Mismatched	0.86 / 0.65	0.88 / 0.68	0.95 / 0.89	0.95 / 0.91	0.80 / 0.56	0.67 / 0.38	0.76 / 0.51

Table 2: AUC / Recall of detecting true set of shifted features in semi-synthetic simulations. Matched refers to when generator and base model are the same, mismatched is when they differ. Results are aggregated across matched and mismatched configurations. Highest performing method is in bold for each dataset and model match setting.

Sample size We evaluate how changing the amount of target domain data available impacts performance in identifying shifted features by subsampling a certain amount of data points in the target domain. Figure 1 shows each method's recall under varying sample sizes and model settings. SGShift outperforms baselines by a large margin regardless the sample size of the dataset or model mismatch, often achieving recall 2 or 3 times higher. With sufficient samples, SGShift-K and SGShift-KA can detect over 90% of the true shifted features, and at any sample size, SGShift with knockoffs achieves top performance. We note that the large confidence intervals are due to aggregating across model settings, and when examining individual model configurations (see appendix), all forms of SGShift nearly always outperform all baselines.

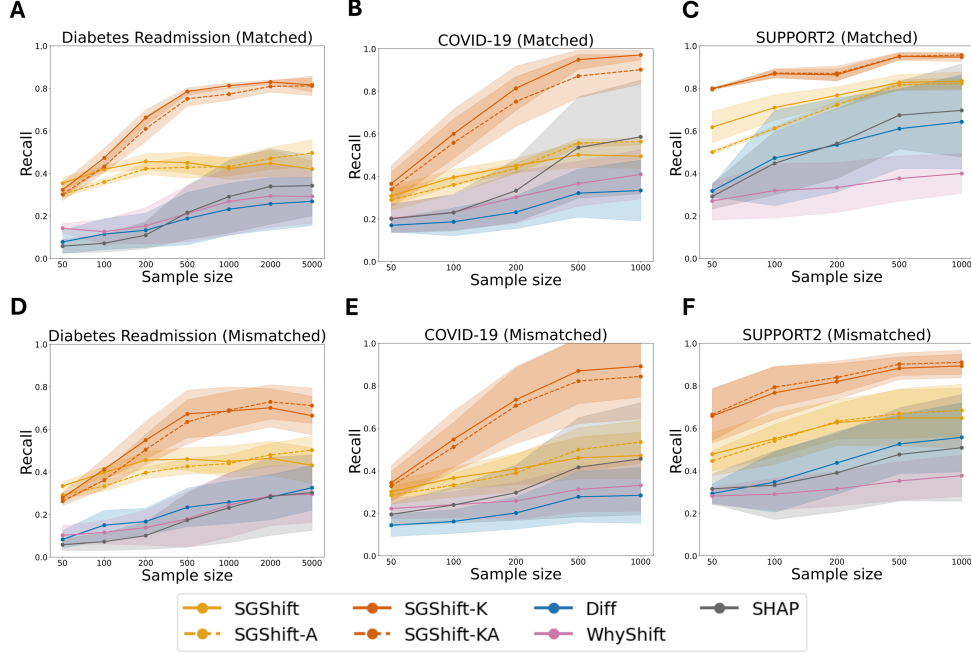


Figure 1: Evaluation of recall at FPR 10% in semi-synthetic simulations for matched and mismatched model settings. Results are aggregated across all model configurations. Standard 95% confidence intervals are shown, calculated as the standard error across model configurations and 100 replicates.

Real-world sparse concept shift We verify the sparsity of true concept shift in Figure 2. We show log loss recovery as the penalty term loosens and more features identified by SGShift are updated in the source model versus models trained only on the source and target datasets. Gradient boosted and regression models are shown as examples in each dataset, and we note the results are similar for all models (see appendix). SGShift recovers a considerable portion of the loss difference between source and target models, and may even improve performance past what the target only model was capable of. This recovery follows an elbow-shape, such that diminishing returns are observed with the incorporation of more features, and performance may even decrease if too many features are added. This indicates the true shift between source and target datasets is indeed often sparse, and only a subset of features are needed to correct for concept shift in real datasets.

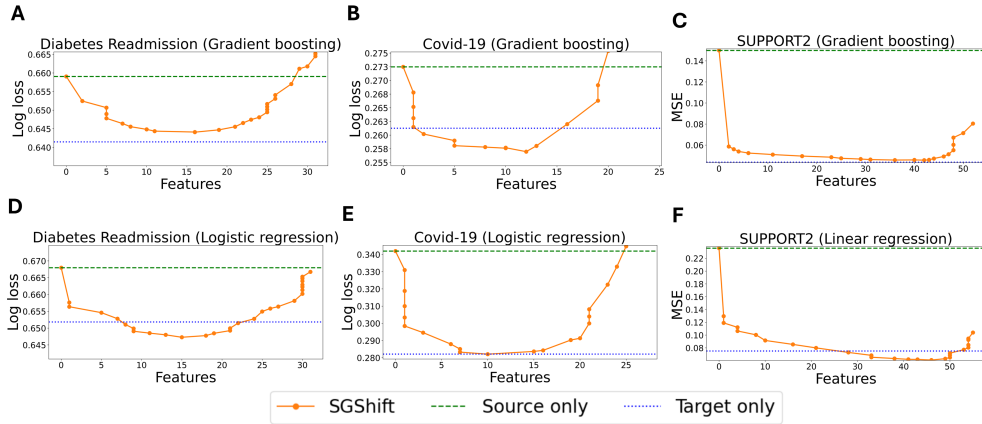


Figure 2: Performance increase as we update more features in the source model identified by SGShift. Each dot represents a penalty between 0 and 1. 2 penalties may have the same number of features selected. Gradient boosting (A, B, C) and logistic/linear regression (D, E, F) are shown as examples in our 3 datasets.

Real-data evaluation We next evaluate the validity of the top features selected by SGShift-KA contributing to the shift in COVID-19 severity after Omicron in Figure 3. The highest ranked feature across all models is respiratory failure with a negative sign, consistent with the broad observation of less severity during Omicron compared to the previous Delta variant [AHM⁺22], partly due to Omicron’s decreased ability at infecting lung cells [HWA⁺23]. More severe cases may be taking place in other pathways, such as the upper respiratory tract [WFP⁺25]. Abnormal breathing and other circulatory/respiratory signs have decreased risk, likely for the same reason. Non-lung related comorbidities tend to contribute more to increased hospitalization risk, as with decreased lung comorbidity risk, they may now be more relevant to severity [LHP⁺22].

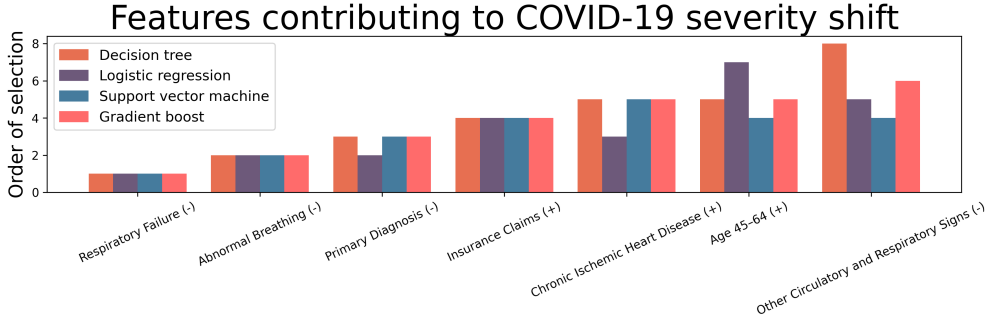


Figure 3: Real data results showing the ordering of selected features for each model as the penalty term increases for COVID-19 severity. Positive (+) and negative (-) coefficients are treated as 2 distinct features. Only features selected in the top 5 for any model are shown.

7 Discussion

We have presented SGShift, a method for attributing concept shift between datasets to a sparse set of features. Our work contributes towards understanding what makes models fail between datasets. We prove statistical guarantees regarding SGShift’s convergence and false discovery control and demonstrate high power in detecting true shifted features. We show that true concept shifts in tabular healthcare data do indeed tend to be sparse and SGShift can explain these shifts. We note that while we assume sparsity, dense concept shifts may exist naturally and be difficult to explain. Future work could include optimizing model performance by explicitly modeling the difference between datasets given the identified shifted features, or extending SGShift to non-tabular data, e.g., images or graphs.

Appendix

Table of contents

- **A.1** Justification of Restricted Strong Convexity
- **A.2** Proof of Theorem 4.1: Convergence Guarantee for Estimation Error Under RSC
- **A.3** Construction and selection with Knockoffs
- **A.4** Proof of Lemma 4.2: Stability Selection Control
- **B** Datasets
- **C** Model Hyperparameters
- **D** Extended Simulation Results
- **E** Extended Real-World Data Results

A.1 Justification of Restricted Strong Convexity (RSC)

The RSC condition is central to ensuring the quadratic growth of the loss difference around the true parameter δ^* , even in high dimensions. We formalize its validity as follows:

Lemma .1 (RSC for ℓ_1 -Penalized Loss). *Let $\phi_i \in \mathbb{R}^K$ be i.i.d. sub-Gaussian vectors with covariance $\Sigma \succ 0$. $L_T(\delta) = \sum_{i=1}^{n_T} \ell(y_i, \hat{f}(X_i) + \phi_i^\top \delta)$, where $\ell(y, \eta)$ is twice-differentiable and $\nabla_\eta^2 \ell(y, \eta) \geq \kappa > 0$ uniformly. We aim to show that, for sufficiently large n_T , with high probability over the sample,*

$$L_T(\mathbf{a}) - L_T(\mathbf{b}) - \langle \mathbf{a} - \mathbf{b}, \nabla L_T(\mathbf{b}) \rangle \geq c_1 n_T \|\mathbf{a} - \mathbf{b}\|_2^2 - c_2 \|\mathbf{a} - \mathbf{b}\|_1^2.$$

for all $\mathbf{a}, \mathbf{b} \in \mathbb{R}^K$, where $c_1, c_2 > 0$ are constants depending on κ and Σ .

Proof. Define $\mathbf{h} = \mathbf{a} - \mathbf{b}$. By Taylor's theorem, there exists a point $\tilde{\delta}$ on the line segment between \mathbf{a} and \mathbf{b} such that

$$L_T(\mathbf{a}) - L_T(\mathbf{b}) - \langle \mathbf{h}, \nabla L_T(\mathbf{b}) \rangle = \frac{1}{2} \mathbf{h}^\top \nabla^2 L_T(\tilde{\delta}) \mathbf{h},$$

where

$$\nabla^2 L_T(\tilde{\delta}) = \sum_{i=1}^{n_T} \nabla_\eta^2 \ell(y_i, \hat{f}(X_i) + \phi_i^\top \tilde{\delta}) \phi_i \phi_i^\top \succeq \kappa \sum_{i=1}^{n_T} \phi_i \phi_i^\top.$$

Defining the empirical covariance $\hat{\Sigma} = \frac{1}{n_T} \sum_{i=1}^{n_T} \phi_i \phi_i^\top$, it follows that

$$\mathbf{h}^\top \nabla^2 L_T(\tilde{\delta}) \mathbf{h} \geq \kappa n_T \mathbf{h}^\top \hat{\Sigma} \mathbf{h}.$$

Under the assumption that $\{\phi_i\}$ are i.i.d. sub-Gaussian with $\mathbb{E}[\phi_i \phi_i^\top] = \Sigma \succ 0$, standard concentration results (e.g., Theorem 9 of [RV10], or Theorem 3.1 in [RWY10]) show that for n_T on the order of $\frac{a \log K}{\lambda_{\min}(\Sigma)}$, the empirical covariance $\hat{\Sigma}$ satisfies a restricted eigenvalue inequality with high probability

$$\mathbf{h}^\top \hat{\Sigma} \mathbf{h} \geq \gamma_{\min} \|\mathbf{h}\|_2^2 - \tau \frac{\log K}{n_T} \|\mathbf{h}\|_1^2.$$

where $\gamma_{\min} > 0$ and $\tau > 0$ are constants depending on Σ and the sub-Gaussian norm of ϕ_i . Combining this restricted eigenvalue (RE) bound with the lower Hessian bound above yields

$$\mathbf{h}^\top \nabla^2 L_T(\tilde{\delta}) \mathbf{h} \geq \kappa n_T \left(\gamma_{\min} \|\mathbf{h}\|_2^2 - \tau \frac{\log K}{n_T} \|\mathbf{h}\|_1^2 \right)$$

Substitute back into the Taylor expansion, there exist constants c_1 and c_2 such that

$$L_T(\mathbf{a}) - L_T(\mathbf{b}) - \langle \mathbf{a} - \mathbf{b}, \nabla L_T(\mathbf{b}) \rangle \geq \underbrace{\frac{1}{2} \kappa \gamma_{\min} n_T}_{c_1} \|\mathbf{a} - \mathbf{b}\|_2^2 - \underbrace{\frac{1}{2} \kappa \tau}_{c_2} \|\mathbf{a} - \mathbf{b}\|_1^2.$$

This is precisely the Restricted Strong Convexity (RSC) condition. \square

A.2 Proof of Theorem 4.1: Convergence Guarantee for Estimation Error Under RSC

Proof. Given the definition of $\hat{\delta}$, there exists a subgradient $\mathbf{z} \in \partial \|\hat{\delta}\|_1$ such that

$$\nabla L(\hat{\delta}) + \lambda \mathbf{z} = \mathbf{0}$$

To bound the norm of the parameter δ , with standard Lasso analysis under Restricted Strong Convexity (RSC) [VdG08], we will use the RSC condition of L that

$$L(\mathbf{a}) - L(\mathbf{b}) - \langle \mathbf{a} - \mathbf{b}, \nabla L(\mathbf{b}) \rangle \geq c_1 n_T \|\mathbf{a} - \mathbf{b}\|_2^2 - c_2 \|\mathbf{a} - \mathbf{b}\|_1^2$$

As $\hat{\delta}$ minimized the penalized loss,

$$L(\hat{\delta}) - L(\delta^*) + \lambda(\|\hat{\delta}\|_1 - \|\delta^*\|_1) \leq 0$$

By the RSC condition

$$L(\hat{\delta}) - L(\delta^*) - \langle \hat{\delta} - \delta^*, \nabla L(\delta^*) \rangle \geq c_1 n_T \|\hat{\delta} - \delta^*\|_2^2 - c_2 \|\hat{\delta} - \delta^*\|_1^2$$

Define $\mathbf{d} = \hat{\delta} - \delta^*$

$$c_1 n_T \|\mathbf{d}\|_2^2 - c_2 \|\mathbf{d}\|_1^2 + \langle \mathbf{d}, \nabla L(\delta^*) \rangle + \lambda(\|\hat{\delta}\|_1 - \|\delta^*\|_1) \leq 0$$

By Hölder's inequality

$$\|\langle \mathbf{d}, \nabla L(\delta^*) \rangle\|_1 \leq \|\mathbf{d}\|_1 \|\nabla L(\delta^*)\|_\infty$$

By triangle inequality

$$\|\hat{\delta}\|_1 - \|\delta^*\|_1 \geq -\|\mathbf{d}\|_1$$

Under the assumption that

$$\begin{aligned} \|\nabla L(\delta^*)\|_\infty &\leq c_3 \lambda \\ |\langle \mathbf{d}, \nabla L(\delta^*) \rangle| &\leq c_3 \lambda \|\mathbf{d}\|_1 \end{aligned}$$

From standard Lasso analysis, we often assume

$$\|\mathbf{d}_{A^c}\|_1 \leq \|\mathbf{d}_A\|_1, \|\mathbf{d}\|_1 \leq 2\|\mathbf{d}_A\|_1$$

By Cauchy-Schwarz inequality

$$\|\mathbf{d}_A\|_1 \leq \sqrt{a} \|\mathbf{d}_A\|_2 \leq \sqrt{a} \|\mathbf{d}\|_2, \|\mathbf{d}\|_1^2 \leq 4a \|\mathbf{d}\|_2^2$$

$$\begin{aligned} 0 &\geq c_1 n_T \|\mathbf{d}\|_2^2 - c_2 \|\mathbf{d}\|_1^2 + \langle \mathbf{d}, \nabla L(\delta^*) \rangle + \lambda(\|\hat{\delta}\|_1 - \|\delta^*\|_1) \\ &\geq c_1 n_T \|\mathbf{d}\|_2^2 - c_2 \|\mathbf{d}\|_1^2 - c_3 \lambda \|\mathbf{d}\|_1 - \lambda \|\mathbf{d}\|_1 \\ &\geq c_1 n_T \|\mathbf{d}\|_2^2 - 4c_2 a \|\mathbf{d}\|_2^2 - 2(c_3 + 1) \sqrt{a} \lambda \|\mathbf{d}\|_2 \\ \|\mathbf{d}\|_2 &\leq \frac{2\sqrt{a}(c_3 + 1)\lambda}{c_1 n_T - 4c_2 a} \end{aligned}$$

with the condition $\lambda \asymp \sqrt{\log K / n_T}$, we can rewrite $\|\mathbf{d}\|_2^2 \leq \frac{Ca \log K}{n_T}$, where $C > 0$ depends on c_1, c_2, c_3 but not on n_T, a , or K , reaching a similar result to [LCL22, LCD23] in sparse high dimensional regression based transfer learning. \square

Remark 1. The RSC condition is ensured by the sub-Gaussian design and curvature of the loss (Lemma .1), which are standard in high-dimensional statistics [RWY10].

Remark 2. Sub-Gaussian concentration gives $\|\nabla L(\delta^*)\|_\infty \leq c_3 \lambda$ with high probability [Ver18].

Remark 3. The condition $\lambda \asymp \sqrt{\log K / n_T}$ ensures compatibility between regularization and noise, standard in ℓ_1 -penalized M-estimation [VdG08].

Remark 4. The offset \hat{f} does not affect RSC because it is fixed during the optimization over δ , leaving the curvature of ℓ and design ϕ_i as the drivers of convexity.

A.3 Construction and selection with Knockoffs

Following [CFJL18], a Model-X knockoff matrix $\tilde{X} = [\tilde{X}^{(1)}, \dots, \tilde{X}^{(p)}] \in \mathbb{R}^{n \times p}$ of a matrix constructed by horizontally stacked random vectors $X = [X^{(1)}, \dots, X^{(p)}] \in \mathbb{R}^{n \times p}$. The knockoffs is constructed such that, for any subset $A \subseteq [p]$,

$$(X, \tilde{X})_{\text{swap}(A)} \stackrel{d}{=} (X, \tilde{X}).$$

where $X^{(j)}$ denotes the j th column of X , $(X, \tilde{X})_{\text{swap}(A)}$ is obtained by swapping the column entries $X^{(j)}$ and $\tilde{X}^{(j)}$ for any $j \in A$. Crucially, \tilde{X} must be constructed conditional on X but independent of y to ensure $\tilde{X} \perp\!\!\!\perp y \mid X$.

We set variable importance measure as coefficients: $Z_k = |\hat{\delta}'_k(\lambda)|$, $\tilde{Z}_k = |\hat{\delta}'_{k+K}(\lambda)|$. Alternatively, we can also use $Z_k = \sup\{\lambda \geq 0 : \hat{\delta}'_k(\lambda) \neq 0\}$, the lambda value where each feature/knockoff enters the lasso path (meaning becomes nonzero). The knockoff filter works by comparing the Z_k 's to the \tilde{Z}_k 's and selecting only variables that are clearly better than their knockoff copy. The reason why this can be done is that, by construction of the knockoffs, the null (not related to y) statistics are pairwise exchangeable. This means that swapping the Z_k and \tilde{Z}_k 's corresponding to null variables leaves the joint distribution of $(Z_1, \dots, Z_K, \tilde{Z}_1, \dots, \tilde{Z}_K)$ unchanged. Once the Z_k and \tilde{Z}_k 's have been computed, different contrast functions can be used to compare them. In general, we must choose an anti-symmetric function h and we compute the symmetrized knockoff statistics $W_k = h(Z_k, \tilde{Z}_k) = -h(\tilde{Z}_k, Z_k)$ such that W_k indicates that X_k appears to be more important than its own knockoff copy. We use difference of absolute values of coefficients by default, but many other alternatives (like signed maximum) are also possible.

Proof of Lemma 4.2: Stability Selection Control

Proof. **PFER Control:** For each null feature $k \in A^c$, the per-iteration selection probability satisfies $P(k \in \hat{A}^{[b]}) \leq \alpha$. This holds if τ is chosen to control the PFER at level αK in each iteration, following [MB10]. Define $V_k^{[b]} = \mathbf{1}\{k \in \hat{A}^{[b]}\}$ as independent Bernoulli trials with $\mathbb{E}[V_k^{[b]}] \leq \alpha$. The selection frequency $\hat{\Pi}_k = \frac{1}{B} \sum_{b=1}^B V_k^{[b]}$ is a binomial proportion with $\mathbb{E}[\hat{\Pi}_k] \leq \alpha$. By Hoeffding's inequality:

$$P\left(\hat{\Pi}_k \geq \pi\right) \leq \exp\left(-2B(\pi - \alpha)^2\right) \quad \forall \pi > \alpha.$$

Summing over all null features and applying linearity of expectation:

$$\mathbb{E}\left[|\hat{A}(\pi) \cap A^c|\right] = \sum_{k \in A^c} P\left(\hat{\Pi}_k \geq \pi\right) \leq |A^c| \exp\left(-2B(\pi - \alpha)^2\right).$$

FDR Control: Let $V^{[b]} = |\hat{A}^{[b]} \cap A^c|$ and $R^{[b]} = |\hat{A}^{[b]}|$. By the knockoff filter guarantee from Theorem 3.1 in [CFJL18], each τ ensures $\mathbb{E}\left[\frac{|\hat{A}^{[b]} \cap A^c|}{|\hat{A}^{[b]}| \vee 1}\right] = \mathbb{E}\left[\frac{V^{[b]}}{R^{[b]} \vee 1}\right] \leq q$. The stabilized FDR satisfies:

$$\begin{aligned} \text{FDR}(\hat{A}(\pi)) &= \mathbb{E}\left[\frac{|\hat{A}(\pi) \cap A^c|}{|\hat{A}(\pi)| \vee 1}\right] \leq \mathbb{E}\left[\frac{\sum_{b=1}^B V^{[b]}}{B\pi}\right] \quad (\text{since } \hat{\Pi}_k \geq \pi \implies \sum_{b=1}^B \mathbf{1}\{k \in \hat{A}^{[b]}\} \geq B\pi) \\ &= \frac{1}{B\pi} \sum_{b=1}^B \mathbb{E}\left[\frac{V^{[b]}}{R^{[b]} \vee 1} \cdot R^{[b]}\right] = \frac{1}{B\pi} \sum_{b=1}^B \mathbb{E}\left[R^{[b]} \cdot \mathbb{E}\left[\frac{V^{[b]}}{R^{[b]} \vee 1} \mid R^{[b]}\right]\right] \\ &\leq \frac{1}{B\pi} \sum_{b=1}^B \mathbb{E}\left[R^{[b]} \cdot q\right] = \frac{q}{B\pi} \sum_{b=1}^B \mathbb{E}\left[R^{[b]}\right]. \end{aligned}$$

where the last line is by Theorem 3.1 in [CFJL18]. From Proposition 1 and Appendix A.2 in [RWC23], the geometric thinning inequality $\sum_{b=1}^B \mathbb{E}[R^{[b]}] \geq \frac{\mathbb{E}[|\hat{A}(\pi)|]}{1 - (1 - \pi)^B}$ holds because each feature's selection events are independent across B iterations. Substituting this bound

$$\text{FDR}(\hat{A}(\pi)) \leq \frac{q}{B\pi} \sum_{b=1}^B \frac{\mathbb{E}[|\hat{A}(\pi)|]}{1 - (1 - \pi)^B} = \frac{q}{1 - (1 - \pi)^B}.$$

□

B Datasets

All datasets are listed as below, and the full preprocessing code from raw data, together with the preprocessed data, are available in the source code, except restricted access COVID-19 Hospitalization data where we provide detailed fetching code and data version information from NIH All of Us Research Program [oURPI19]. Standardization is performed within the pipeline to ensure that features with larger values don't disproportionately influence the ℓ_1 regularization penalty.

Diabetes 30-Day Readmission The Diabetes 130-US Hospitals dataset, available through the UCI Machine Learning Repository (<https://archive.ics.uci.edu/dataset/296/diabetes+130-us+hospitals+for+years+1999-2008>), comprises 101,766 encounters of diabetic patients across 130 U.S. hospitals between 1999-2008 [SDG⁺14]. We fetch the data following TableShift's procedure [GPS23]. We define the source domain as 49,213 non-ER admissions (elective or urgent) with 25,196 readmitted patients, and the target domain as 24,402 ER admissions with 10,684 readmitted patients, with the binary classification task being prediction of 30-day readmission risk.

COVID-19 Hospitalization The COVID-19 cohort is part of the NIH All of Us Research Program [oURPI19], a (restricted access) dataset containing electronic health records for 16,187 patients diagnosed with COVID-19 between 2020-2022. Features include demographic variables (age, gender, race), temporal indicators (diagnosis date relative to Omicron variant emergence), comorbidity status for 13 chronic conditions (diabetes, COPD), and diagnostic context (EHR vs. claims-based). We partition the data into three temporal groups: a source domain of 11,268 patients diagnosed prior to the beginning of 2022 with 2,541 patients hospitalized, a target domain of 2,219 patients diagnosed in January 2022 (early Omicron era) with 359 patients hospitalized. The binary classification task predicts hospitalization status (inpatient vs. outpatient).

SUPPORT2 Hospital Charges From the Study to Understand Prognoses Preferences Outcomes and Risks of Treatment (SUPPORT2), publicly available via the UCI repository (<https://archive.ics.uci.edu/dataset/880/support2>) containing 9,105 critically ill patients [CDD⁺95]. The source domain is specified as 5,453 patients who survived hospitalization and the target domain as 1,817 in-hospital deaths. The regression task is defined as a prediction of $\log_{10}(\text{total hospital costs per patient})$.

C Model Hyperparameters

We used standard implementations of classical machine learning models from `scikit-learn`, with hyperparameters either set to commonly used defaults or manually tuned for stability and performance. Supplementary table 3 summarizes the key hyperparameters for each model. Unless otherwise stated, all models were trained using their default solver settings. Random seeds were fixed via `random_state` to ensure reproducibility.

Model	Hyperparameters
Decision Tree (Classifier)	<code>max_depth=4, random_state={seed}</code>
Support Vector Machine (Classifier)	<code>kernel='rbf', C=1.0, probability=True, random_state={seed}</code>
Gradient Boosting Classifier	<code>n_estimators=100, random_state={seed}</code>
Logistic Regression	<code>max_iter=200, random_state={seed}</code>
Decision Tree (Regressor)	<code>max_depth=4, random_state={seed}</code>
Support Vector Machine (Regressor)	<code>kernel='rbf', C=1.0</code>
Linear Regression	default settings
Gradient Boosting Regressor	<code>n_estimators=100, random_state={seed}</code>

Table 3: Hyperparameters used for each model. The same random seed (`{seed}`) was applied across models where applicable to ensure consistency.

D Extended Simulation Results

Table 4: Diabetes readmission semi-synthetic simulations. AUC is shown for each generator and base model configuration. DT = decision tree, GB = gradient boosting, LR = logistic regression, SVM = support vector machine.

Generator	Base	SGShift	SGShift-A	SGShift-K	SGShift-KA	Diff	WhyShift	SHAP
DT	DT	0.77	0.75	0.91	0.92	0.47	0.62	0.53
	GB	0.82	0.83	0.90	0.91	0.69	0.65	0.78
	LR	0.80	0.83	0.86	0.86	0.74	0.70	0.81
	SVM	0.78	0.79	0.85	0.88	0.71	0.62	0.75
GB	DT	0.78	0.80	0.85	0.86	0.61	0.77	0.63
	GB	0.82	0.83	0.90	0.92	0.70	0.79	0.82
	LR	0.77	0.78	0.81	0.84	0.74	0.80	0.87
	SVM	0.81	0.81	0.86	0.87	0.76	0.80	0.89
LR	DT	0.76	0.83	0.83	0.86	0.64	0.67	0.59
	GB	0.85	0.85	0.86	0.88	0.71	0.77	0.79
	LR	0.79	0.83	0.88	0.87	0.72	0.79	0.87
	SVM	0.78	0.81	0.86	0.89	0.70	0.79	0.86
SVM	DT	0.83	0.79	0.84	0.84	0.61	0.63	0.62
	GB	0.81	0.82	0.83	0.84	0.69	0.70	0.77
	LR	0.73	0.76	0.76	0.80	0.69	0.72	0.79
	SVM	0.81	0.82	0.89	0.89	0.66	0.72	0.84

Table 5: COVID-19 semi-synthetic simulations. AUC is shown for each generator and base model configuration. DT = decision tree, GB = gradient boosting, LR = logistic regression, SVM = support vector machine.

Generator	Base	SGShift	SGShift-A	SGShift-K	SGShift-KA	Diff	WhyShift	SHAP
DT	DT	0.82	0.85	0.98	0.89	0.60	0.59	0.48
	GB	0.84	0.86	0.96	0.94	0.74	0.59	0.66
	LR	0.79	0.81	0.85	0.80	0.75	0.59	0.63
	SVM	0.80	0.83	0.93	0.89	0.66	0.54	0.56
GB	DT	0.84	0.89	0.99	0.98	0.69	0.72	0.68
	GB	0.90	0.89	1.00	0.99	0.84	0.84	0.94
	LR	0.81	0.82	0.99	0.96	0.85	0.81	0.96
	SVM	0.84	0.88	0.99	0.99	0.83	0.79	0.92
LR	DT	0.85	0.89	0.97	0.97	0.66	0.70	0.66
	GB	0.92	0.91	0.99	0.98	0.85	0.79	0.90
	LR	0.86	0.87	0.99	0.95	0.84	0.84	0.95
	SVM	0.87	0.89	0.99	0.99	0.84	0.74	0.86
SVM	DT	0.84	0.88	0.98	0.97	0.67	0.67	0.62
	GB	0.92	0.91	0.99	0.98	0.84	0.81	0.90
	LR	0.83	0.84	0.97	0.96	0.83	0.82	0.93
	SVM	0.87	0.89	0.99	0.99	0.83	0.76	0.87

Table 6: SUPPORT2 semi-synthetic simulations. AUC is shown for each generator and base model configuration. DT = decision tree, GB = gradient boosting, LR = linear regression, SVM = support vector machine.

Generator	Base	SGShift	SGShift-A	SGShift-K	SGShift-KA	Diff	WhyShift	SHAP
DT	DT	0.93	0.94	0.97	0.97	0.67	0.63	0.54
	GB	0.89	0.90	0.98	0.98	0.84	0.68	0.92
	LR	0.80	0.80	0.93	0.93	0.78	0.62	0.69
	SVM	0.84	0.85	0.95	0.94	0.73	0.60	0.68
GB	DT	0.89	0.89	0.96	0.96	0.66	0.64	0.64
	GB	0.92	0.93	0.96	0.96	0.85	0.71	0.94
	LR	0.81	0.81	0.93	0.92	0.83	0.64	0.73
	SVM	0.86	0.86	0.96	0.96	0.80	0.61	0.70
LR	DT	0.81	0.88	0.92	0.96	0.68	0.66	0.66
	GB	0.86	0.89	0.93	0.96	0.86	0.73	0.80
	LR	0.93	0.95	0.96	0.96	0.97	0.73	0.96
	SVM	0.86	0.87	0.95	0.96	0.83	0.67	0.73
SVM	DT	0.92	0.94	0.96	0.96	0.68	0.71	0.68
	GB	0.92	0.94	0.96	0.96	0.88	0.71	0.95
	LR	0.92	0.93	0.96	0.95	0.96	0.73	0.94
	SVM	0.92	0.94	0.95	0.96	0.84	0.61	0.82

Table 7: Diabetes readmission semi-synthetic simulations. Recall is shown for each generator and base model configuration. DT = decision tree, GB = gradient boosting, LR = logistic regression, SVM = support vector machine.

Generator	Base	SGShift	SGShift-A	SGShift-K	SGShift-KA	Diff	WhyShift	SHAP
DT	DT	0.41	0.39	0.85	0.83	0.08	0.14	0.12
	GB	0.47	0.51	0.74	0.77	0.14	0.22	0.17
	LR	0.38	0.50	0.60	0.56	0.39	0.28	0.23
	SVM	0.38	0.41	0.67	0.71	0.36	0.16	0.18
GB	DT	0.37	0.50	0.76	0.73	0.15	0.41	0.20
	GB	0.48	0.54	0.83	0.86	0.29	0.46	0.38
	LR	0.37	0.44	0.64	0.67	0.44	0.55	0.65
	SVM	0.45	0.50	0.71	0.73	0.47	0.48	0.62
LR	DT	0.37	0.53	0.57	0.80	0.21	0.23	0.17
	GB	0.58	0.65	0.76	0.81	0.39	0.35	0.38
	LR	0.41	0.54	0.77	0.74	0.38	0.37	0.52
	SVM	0.37	0.51	0.74	0.78	0.39	0.40	0.51
SVM	DT	0.54	0.51	0.65	0.73	0.24	0.13	0.16
	GB	0.56	0.57	0.70	0.70	0.35	0.16	0.18
	LR	0.32	0.40	0.44	0.53	0.38	0.18	0.19
	SVM	0.37	0.51	0.81	0.82	0.32	0.20	0.35

Table 8: COVID-19 semi-synthetic simulations. Recall is shown for each generator and base model configuration. DT = decision tree, GB = gradient boosting, LR = logistic regression, SVM = support vector machine.

Generator	Base	SGShift	SGShift-A	SGShift-K	SGShift-KA	Diff	WhyShift	SHAP
DT	DT	0.41	0.56	0.93	0.79	0.10	0.25	0.15
	GB	0.45	0.51	0.88	0.85	0.10	0.23	0.14
	LR	0.36	0.39	0.45	0.22	0.20	0.15	0.18
	SVM	0.39	0.44	0.76	0.70	0.12	0.11	0.09
GB	DT	0.39	0.51	0.98	0.94	0.20	0.32	0.30
	GB	0.56	0.58	0.99	0.96	0.35	0.51	0.76
	LR	0.36	0.41	0.97	0.89	0.42	0.48	0.88
	SVM	0.42	0.54	0.98	0.97	0.34	0.37	0.69
LR	DT	0.49	0.57	0.92	0.91	0.15	0.33	0.30
	GB	0.70	0.73	0.96	0.95	0.45	0.46	0.64
	LR	0.50	0.54	0.98	0.92	0.47	0.53	0.84
	SVM	0.52	0.59	0.98	0.95	0.42	0.31	0.56
SVM	DT	0.44	0.56	0.94	0.91	0.19	0.27	0.23
	GB	0.69	0.70	0.96	0.93	0.42	0.48	0.70
	LR	0.44	0.46	0.92	0.89	0.42	0.46	0.78
	SVM	0.51	0.58	0.97	0.95	0.41	0.35	0.60

Table 9: SUPPORT2 semi-synthetic simulations. Recall is shown for each generator and base model configuration. DT = decision tree, GB = gradient boosting, LR = linear regression, SVM = support vector machine.

Generator	Base	SGShift	SGShift-A	SGShift-K	SGShift-KA	Diff	WhyShift	SHAP
DT	DT	0.87	0.84	0.97	0.97	0.32	0.33	0.36
	GB	0.71	0.72	0.94	0.94	0.64	0.42	0.84
	LR	0.44	0.45	0.82	0.76	0.50	0.23	0.11
	SVM	0.59	0.64	0.88	0.88	0.39	0.25	0.33
GB	DT	0.71	0.73	0.93	0.94	0.32	0.34	0.52
	GB	0.76	0.78	0.96	0.96	0.65	0.48	0.86
	LR	0.43	0.46	0.86	0.82	0.55	0.28	0.16
	SVM	0.62	0.62	0.94	0.94	0.52	0.28	0.37
LR	DT	0.48	0.71	0.76	0.93	0.40	0.38	0.54
	GB	0.65	0.71	0.88	0.93	0.68	0.51	0.63
	LR	0.87	0.85	0.93	0.95	0.94	0.51	0.92
	SVM	0.63	0.67	0.92	0.94	0.55	0.37	0.30
SVM	DT	0.84	0.84	0.94	0.95	0.44	0.47	0.58
	GB	0.84	0.84	0.93	0.94	0.77	0.48	0.90
	LR	0.84	0.82	0.92	0.94	0.92	0.51	0.82
	SVM	0.84	0.82	0.92	0.94	0.66	0.29	0.65

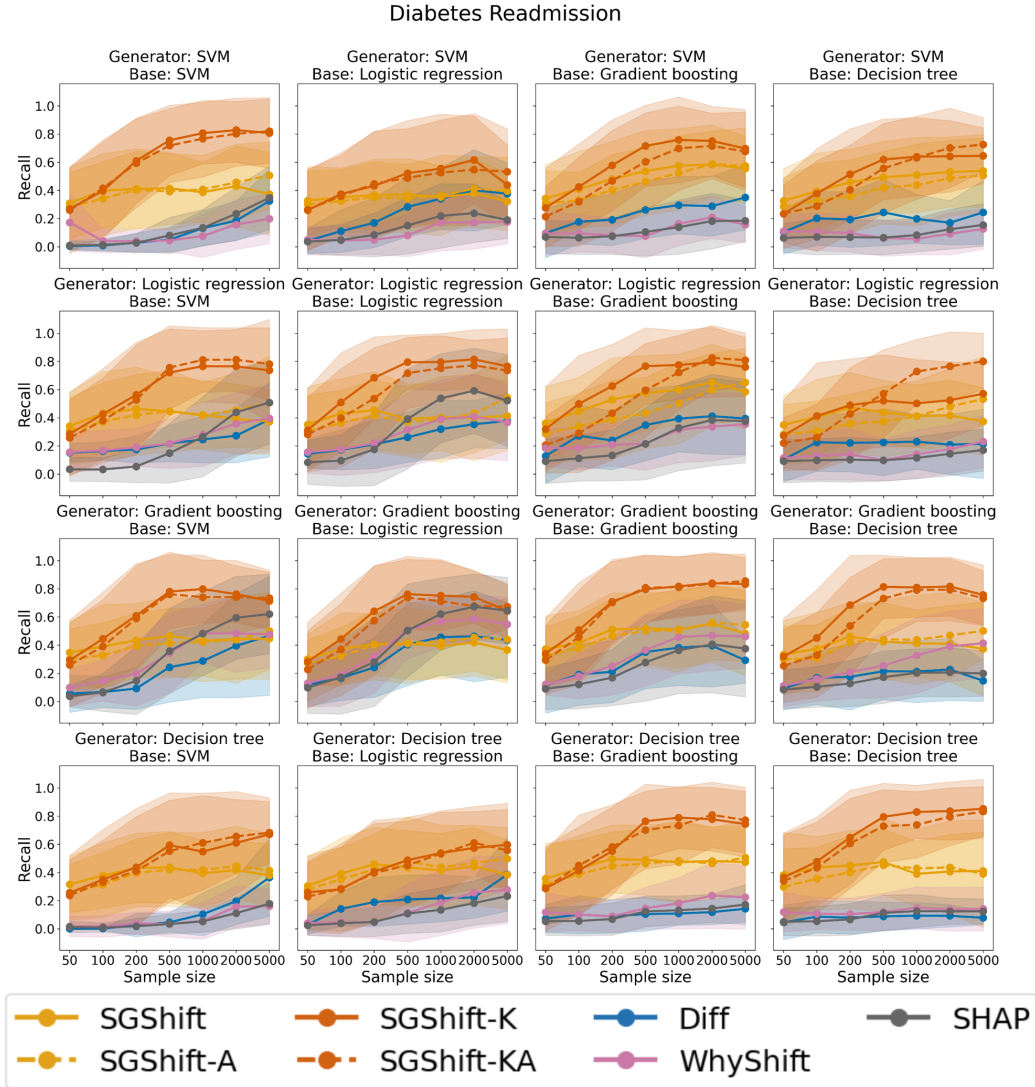


Figure 4: Individual model configuration results for diabetes readmission semi-synthetic simulations, measured in recall. 2 standard error intervals are shown over 100 replicates.

COVID-19

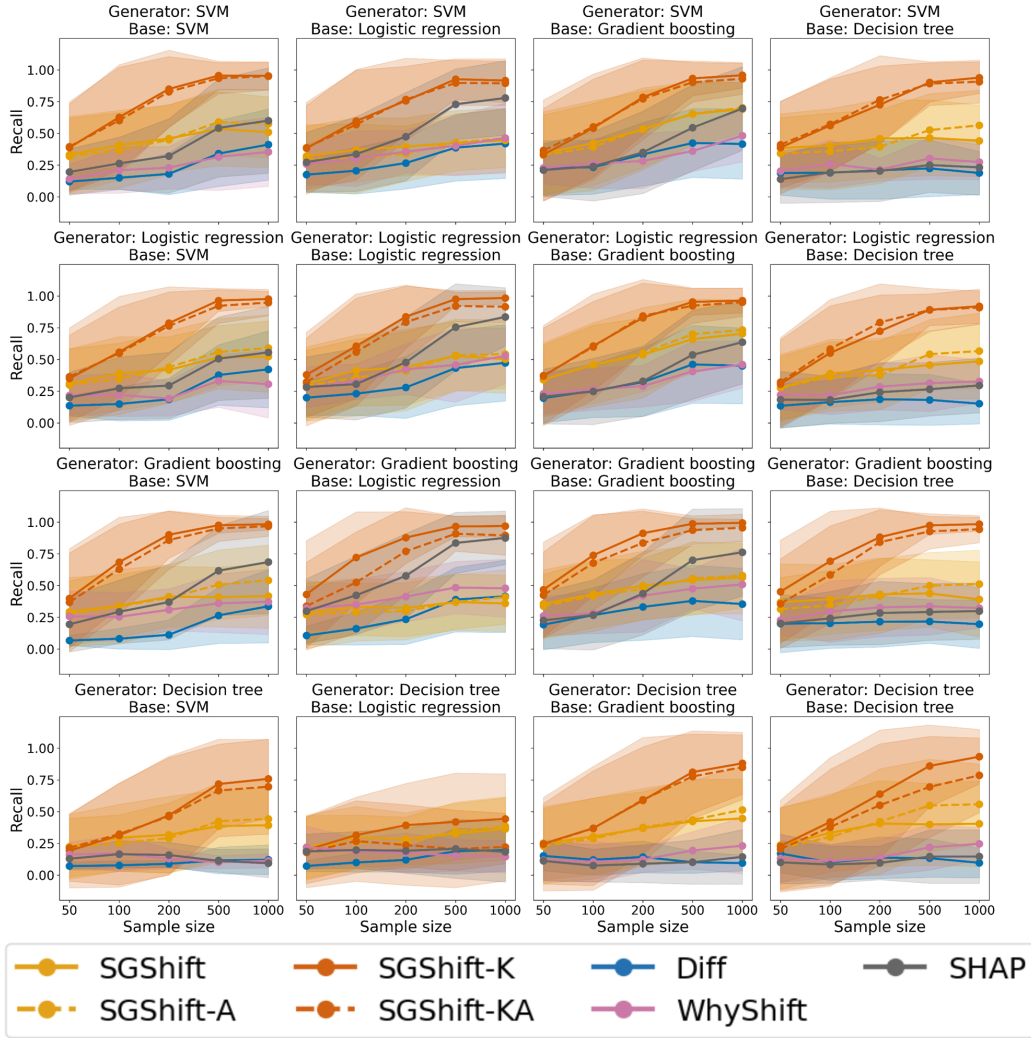


Figure 5: Individual model configuration results for COVID-19 semi-synthetic simulations, measured in recall. 2 standard error intervals are shown over 100 replicates.

SUPPORT2

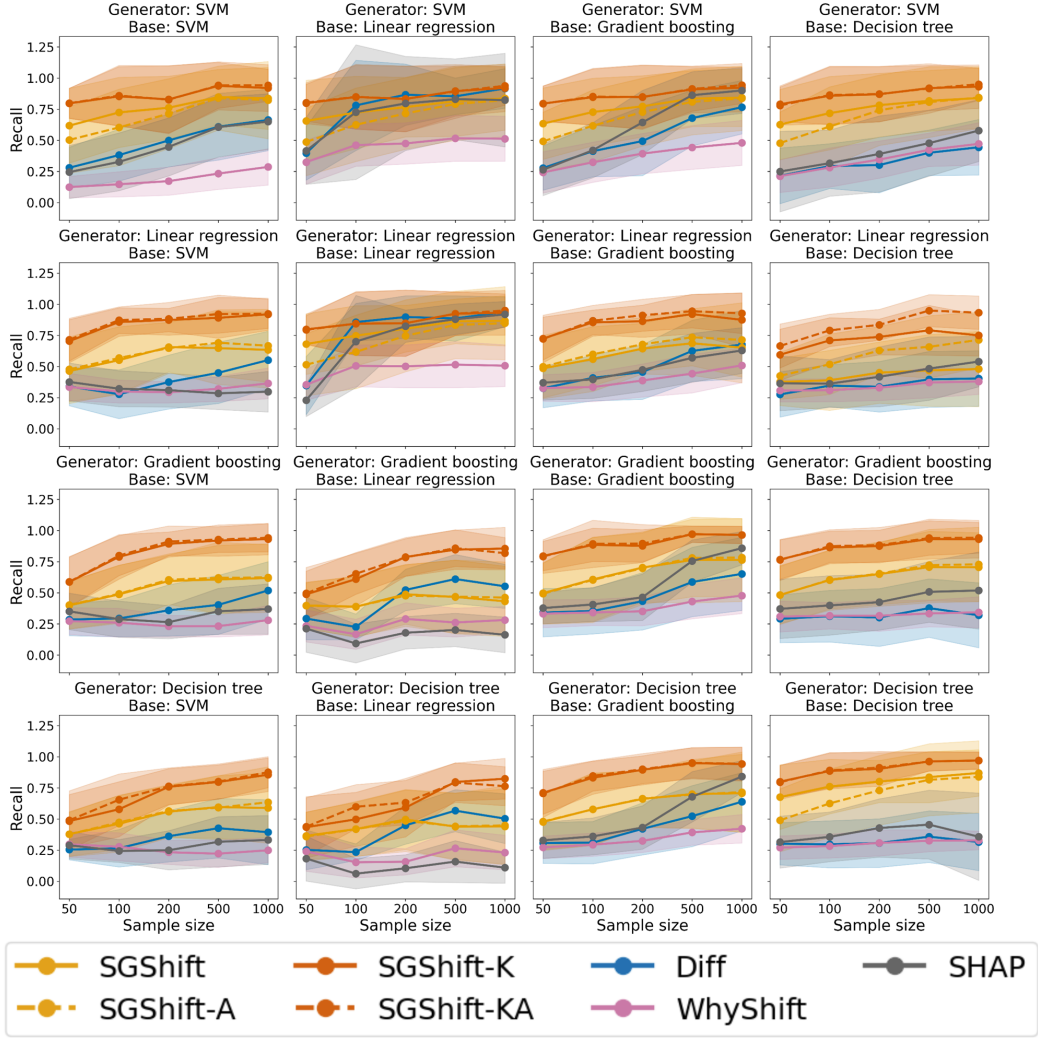


Figure 6: Individual model configuration results for SUPPORT2 semi-synthetic simulations, measured in recall. 2 standard error intervals are shown over 100 replicates.

E Extended Real-World Data Results

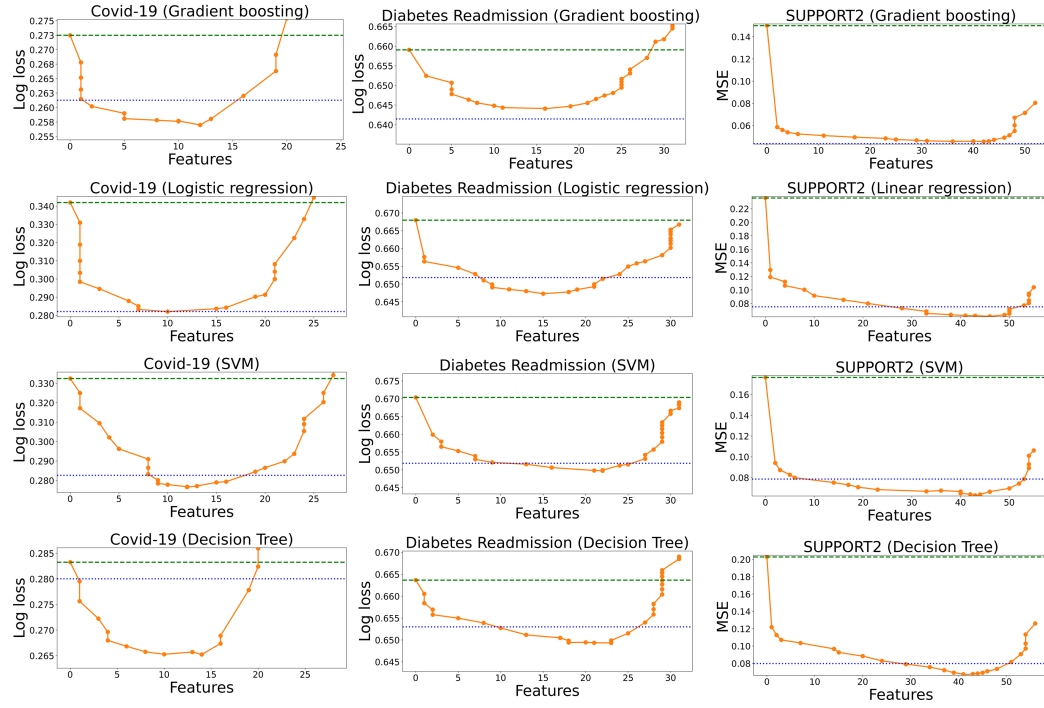


Figure 7: Performance increase as we update more features in the source model identified by SGShift. Each dot represents a penalty between 0 and 1. 2 penalties may have the same number of features selected.

References

- [AHM⁺22] Solomon Adjei, Kai Hong, Nicole M Molinari, et al. Mortality risk among patients hospitalized primarily for covid-19 during the omicron and delta variant pandemic periods — united states, april 2020–june 2022. *MMWR Morbidity and Mortality Weekly Report*, 71:1182–1189, 2022.
- [CDD⁺95] Alfred F Connors, Neal V Dawson, Norman A Desbiens, William J Fulkerson, Lee Goldman, William A Knaus, Joanne Lynn, Robert K Oye, Marilyn Bergner, Anne Damiano, et al. A controlled trial to improve care for seriously iii hospitalized patients: The study to understand prognoses and preferences for outcomes and risks of treatments (support). *Jama*, 274(20):1591–1598, 1995.
- [CFJL18] Emmanuel Candes, Yingying Fan, Lucas Janson, and Jinchi Lv. Panning for gold: ‘model-x’ knockoffs for high dimensional controlled variable selection. *Journal of the Royal Statistical Society Series B: Statistical Methodology*, 80(3):551–577, 2018.
- [CNY23] Tiffany Tianhui Cai, Hongseok Namkoong, and Steve Yadlowsky. Diagnosing model performance under distribution shift. *arXiv preprint arXiv:2303.02011*, 2023.
- [CZZ22] Lingjiao Chen, Matei Zaharia, and James Y Zou. Estimating and explaining model performance when both covariates and labels shift. *Advances in Neural Information Processing Systems*, 35:11467–11479, 2022.
- [GMR⁺18] Riccardo Guidotti, Anna Monreale, Salvatore Ruggieri, Franco Turini, Fosca Giannotti, and Dino Pedreschi. A survey of methods for explaining black box models. *ACM computing surveys (CSUR)*, 51(5):1–42, 2018.
- [GPS23] Josh Gardner, Zoran Popovic, and Ludwig Schmidt. Benchmarking distribution shift in tabular data with tableshift. *Advances in Neural Information Processing Systems*, 2023.
- [Has17] Trevor J Hastie. Generalized additive models. *Statistical models in S*, pages 249–307, 2017.
- [HWA⁺23] Markus Hoffmann, Lanying YR Wong, Prerna Arora, et al. Omicron subvariant ba.5 efficiently infects lung cells. *Nature Communications*, 14:3500, 2023.
- [JPLB22] Sooyong Jang, Sangdon Park, Insup Lee, and Osbert Bastani. Sequential covariate shift detection using classifier two-sample tests. In *International conference on machine learning*, pages 9845–9880. PMLR, 2022.
- [KBI20] Sean Kulinski, Saurabh Bagchi, and David I Inouye. Feature shift detection: Localizing which features have shifted via conditional distribution tests. *Advances in neural information processing systems*, 33:19523–19533, 2020.
- [KI23] Sean Kulinski and David I Inouye. Towards explaining distribution shifts. In *International Conference on Machine Learning*, pages 17931–17952. PMLR, 2023.
- [LCD23] Sai Li, Tianxi Cai, and Rui Duan. Targeting underrepresented populations in precision medicine: A federated transfer learning approach. *The annals of applied statistics*, 17(4):2970, 2023.
- [LCL22] Sai Li, T Tony Cai, and Hongzhe Li. Transfer learning for high-dimensional linear regression: Prediction, estimation and minimax optimality. *Journal of the Royal Statistical Society Series B: Statistical Methodology*, 84(1):149–173, 2022.
- [LHP⁺22] Joseph A Lewnard, Vincent X Hong, Manish M Patel, et al. Clinical outcomes associated with sars-cov-2 omicron (b.1.1.529) variant and ba.1/ba.1.1 or ba.2 subvariant infection in southern california. *Nature Medicine*, 28:1933–1943, 2022.
- [LWCN23] Jiashuo Liu, Tianyu Wang, Peng Cui, and Hongseok Namkoong. On the need for a language describing distribution shifts: Illustrations on tabular datasets. *Advances in Neural Information Processing Systems*, 36:51371–51408, 2023.

- [LWCN24] Jiashuo Liu, Tianyu Wang, Peng Cui, and Hongseok Namkoong. Rethinking distribution shifts: Empirical analysis and inductive modeling for tabular data, 2024.
- [LWS18] Zachary Lipton, Yu-Xiang Wang, and Alexander Smola. Detecting and correcting for label shift with black box predictors. In *International conference on machine learning*, pages 3122–3130. PMLR, 2018.
- [MB10] Nicolai Meinshausen and Peter Bühlmann. Stability selection. *Journal of the Royal Statistical Society Series B: Statistical Methodology*, 72(4):417–473, 2010.
- [MBM⁺23] Carlos Mougan, Klaus Broelemann, David Masip, Gjergji Kasneci, Thanassis Thiropanis, and Steffen Staab. Explanation shift: How did the distribution shift impact the model? *arXiv preprint arXiv:2303.08081*, 2023.
- [MDSR25] Hayden McTavish, Jon Donnelly, Margo Seltzer, and Cynthia Rudin. Interpretable generalized additive models for datasets with missing values. *Advances in Neural Information Processing Systems*, 37:11904–11945, 2025.
- [oURPI19] All of Us Research Program Investigators. The “all of us” research program. *New England Journal of Medicine*, 381(7):668–676, 2019.
- [RV10] Mark Rudelson and Roman Vershynin. Non-asymptotic theory of random matrices: extreme singular values. In *Proceedings of the International Congress of Mathematicians 2010 (ICM 2010) (In 4 Volumes) Vol. I: Plenary Lectures and Ceremonies Vols. II–IV: Invited Lectures*, pages 1576–1602. World Scientific, 2010.
- [RWC23] Zhimei Ren, Yuting Wei, and Emmanuel Candès. Derandomizing knockoffs. *Journal of the American Statistical Association*, 118(542):948–958, 2023.
- [RWY10] Garvesh Raskutti, Martin J Wainwright, and Bin Yu. Restricted eigenvalue properties for correlated gaussian designs. *The Journal of Machine Learning Research*, 11:2241–2259, 2010.
- [SDG⁺14] Beata Strack, Jonathan P DeShazo, Chris Gennings, Juan L Olmo, Sebastian Ventura, Krzysztof J Cios, and John N Clore. Impact of hba1c measurement on hospital readmission rates: analysis of 70,000 clinical database patient records. *BioMed research international*, 2014(1):781670, 2014.
- [SKM07] Masashi Sugiyama, Matthias Krauledat, and Klaus-Robert Müller. Covariate shift adaptation by importance weighted cross validation. *Journal of Machine Learning Research*, 8(5), 2007.
- [VdG08] Sara A Van de Geer. High-dimensional generalized linear models and the lasso. 2008.
- [Ver18] Roman Vershynin. *High-dimensional probability: An introduction with applications in data science*, volume 47. Cambridge university press, 2018.
- [WFP⁺25] A. Wickenhagen, M. Flagg, J.R. Port, et al. Evolution of omicron lineage towards increased fitness in the upper respiratory tract in the absence of severe lung pathology. *Nature Communications*, 16:594, 2025.
- [ZSGJ23] Haoran Zhang, Harvineet Singh, Marzyeh Ghassemi, and Shalmali Joshi. " why did the model fail?": Attributing model performance changes to distribution shifts. 2023.